Carrier-induced disordering dynamics in InSb studied with density functional perturbation theory

P. B. Hillyard,[1,2] D. A. Reis,[3,2] and K. J. Gaffney[2,*]
[1]*Department of Chemistry, Stanford University, Stanford, California 94305, USA*
[2]*PULSE Center, Stanford Linear Accelerator Center, Stanford University, Stanford, California 94305, USA*
[3]*FOCUS Center, Department of Physics and Applied Physics Program, University of Michigan, Ann Arbor, Michigan 48109, USA*
(Received 6 February 2008; published 28 May 2008)

Density functional perturbation theory calculations have been utilized to characterize the carrier density dependent phonon dispersion of InSb. Similar to prior theoretical studies of Si, these calculations predict that a shear instability develops in the crystal at a carrier density of 3.7% of the valence electron density and the entire transverse acoustic phonon branch becomes unstable over a narrow carrier density range of roughly 1%. Unlike calculations for Si, the shear instability appears first at the *X* point, rather than the *L* point. We utilize these calculations to interpret recent ultrafast x-ray diffraction measurements of laser-induced disordering in InSb and find that the time scale and laser fluence dependence of the measured disordering dynamics are consistent with these theoretical predictions. The calculations, however, do not reproduce the experimental anisotropy in the root-mean-square displacement.

DOI: 10.1103/PhysRevB.77.195213 PACS number(s): 78.47.−p, 63.20.−e, 78.70.Ck, 71.15.Mb

I. INTRODUCTION

Ultrafast laser excitation above the electronic band gap can deposit substantial amounts of energy per unit cell in a time short compared to the time required for energy equilibration between the electronic and vibrational degrees of freedom. Such excitation processes present the opportunity to investigate the influence of electronic excitation on the topology of interatomic potential energy surfaces prior to energy dissipation to the lattice.

Extensive experimental studies with intense femtosecond duration laser pulses have investigated the operative mechanism for crystal melting under different excitation conditions. Intense femtosecond pulse excitation of the tetrahedrally bonded semiconductors C,[1,2] GaAs,[3–12] InSb,[13] and Si,[3,14,15] leads to large changes in the linear and second harmonic reflectivity that develop on a subpicosecond time scale. Although absorption of the laser generates an increased reflectivity due to the direct excitation of carriers, the magnitude of the observed change cannot be explained by this effect alone, which leads to the conclusion that intense laser excitation causes a semiconductor to metal transition. Since Si, Ge, GaAs, and InSb form metallic liquids, metallic reflectivities have been attributed to crystal melting.[16] The rate of this purported phase transition exceeds the expected rate for energy transfer from the excited electrons to the crystal vibrations, which leads to the supposition that the melting occurs nonthermally. Despite these extensive investigations, uncertainty about the melting mechanism persists largely because an optical probe interrogates the electronic structure, and information about the atomic structure must be indirectly inferred.

An extensive variety of theoretical methods has also been utilized to investigate the properties of semiconductor crystals with electronic temperatures orders of magnitude larger than the vibrational temperatures. Multiple theoretical studies have predicted that a shear instability develops in tetrahedrally bonded semiconductors at extreme electronic temperatures, which could lead to spontaneous crystal disordering and melting without the need for vibrational excitation. Biswas and Ambegaokar, using a bond charge model, demonstrated that the transverse acoustic phonon modes in Si significantly soften with excitation of a few percent of the valence electron density into the conduction band.[17] This softening eventually leads to a shear instability, with the transverse acoustic phonon frequency at the *L* point becoming imaginary at a carrier density of 4.5%. Further increases in carrier density lead to destabilization of the transverse acoustic modes over the entire Brillouin zone. Stampfli and Bennemann performed a series of theoretical investigations on silicon by using a tight binding formalism that also predicted a carrier driven shear instability.[18–20] While stimulating and provocative, the applicability of these calculations to the conditions generated by intense femtosecond duration pulses has been difficult to determine.[21] Recoules *et al.*[22] recently performed calculations on lattice stability within the density functional framework and achieved results consistent with the work outlined above. Molecular dynamics simulations by Dumitrica *et al.*[23,24] implicated electronic excitation to destabilization of covalent bonds, leading to loss of order in the material and a laser-induced phase transition. On the other hand, the quantum molecular dynamics simulations of Silvistrelli *et al.*[25,26] showed that silicon melts on the subpicosecond time scale without an electronically generated mechanical instability, even when the initial electronic temperature exceeds the vibrational temperature by nearly 2 orders of magnitude.

This puzzling situation made nonthermal melting a natural phenomenon to investigate with ultrafast x-ray diffraction due to its sensitivity to atomic structure.[27,28] Initial studies performed with laser plasma generated femtosecond x-ray pulses observed a large amplitude subpicosecond decay of the (111) Bragg peak for both InSb (Ref. 29) and Ge.[30] These measurements provided the first direct experimental evidence that large scale atomic disordering proceeds concurrently with the large increase in optical reflectivity, but the

subpicosecond time scale alone does not confirm that disordering occurs via a carrier generated shear instability due to the conflicting simulation results of Silvistrelli *et al.*[25,26]

The Sub-Picosecond Pulse Source (SPPS) collaboration at the Stanford Linear Accelerator Center (SLAC) used the SLAC linear electron accelerator to generate a femtosecond x-ray source that is significantly brighter than laser plasma based sources. The superior characteristics of the SPPS x-ray source allowed laser initiated disordering dynamics to be studied with unprecedented detail. The experiments at the SPPS produced a series of unexpected observations, which we will briefly summarize. The first of these studies, reported by Lindenberg *et al.*,[31] extracted a time-dependent root-mean-square (rms) displacement from the time-resolved diffraction intensity. Under intense laser excitation conditions, they observed that the rms displacement increases linearly for many hundreds of femtoseconds for both the (111) and the (220) Bragg peaks. The average velocity of the atoms extracted from the slope of the time-dependent rms displacement projected onto the ⟨111⟩ and ⟨110⟩ directions is equal to the room temperature rms velocity of InSb, which is indicative of constant velocity, inertial dynamics. The observation of angstrom length scale increases in the rms displacements without a significant increase in the atomic velocities represents definitive experimental evidence that electronic excitation significantly modifies the shape of the interatomic potential energy surface prior to large scale phonon excitation. The subsequent study reported by Gaffney *et al.*[32] showed that after the first half picosecond, the rms displacement increases faster for projections in the ⟨111⟩ direction than in the ⟨110⟩ direction. While anisotropy had been predicted for Si and GaAs,[17,20] these theories predicted faster disordering in the ⟨110⟩ direction, in direct opposition to the findings of Gaffney *et al.*[32] The third set of measurements performed by Hillyard *et al.*[33] at the SPPS measured the disordering dynamics over a large carrier density range and observed the onset of lattice softening and the appearance of accelerated atomic displacements. This provided experimental evidence of accelerated disordering on an unstable potential energy surface, which had been predicted by theory. However, the predominance of inertial dynamics over a wide range of laser fluence appears in conflict with the theoretically predicted sensitivity of the interatomic potential of similar materials to small increases in carrier density once a carrier density sufficient for significant lattice softening has been achieved.

Transforming these experimental observations into a detailed atomic scale understanding of the mechanism for melting in the presence of a dense electron-hole plasma has been impeded by the apparent discrepancies between theory and experiment. The previous theoretical studies did not include InSb and were not able to benefit from modern advances in theoretical methods with the exception of the study by Recoules *et al.* However, this study was limited to studying the lattice stability of silicon at two carrier density points.[22] These advances present other opportunities for *ab initio* investigations and the opportunity to better characterize experiment and potentially alleviate the discrepancies between theory and experiment previously discussed. We calculate the carrier density dependent phonon dispersion curves by using *ab initio* density functional perturbation theory[34–36] (DFPT) to clarify the impact of electronic excitation on InSb lattice stability. A method for determining the time-dependent rms displacements and diffraction intensities from the calculated carrier-dependent lattice dynamics has been developed to assist comparison between calculation and experiment. This paper presents the results of these calculations and their comparison to experimental findings previously published.

II. CALCULATIONAL METHODS

Electronic structure and lattice dynamics calculations are performed by using density functional perturbation theory[34–36] as implemented in the ABINIT code,[37] which is a common project of the Université Catholique de Louvain, Corning Incorporated, and other contributors.[37,63] Excited carriers are generated by applying a finite temperature to a Fermi–Dirac distribution for the electronic system with the lattice constant fixed, establishing thermal equilibrium between the electrons and holes, but not with the lattice. These calculations utilize a single chemical potential for both electrons and holes,[22,38,39] unlike the work of Fahy and coworkers for Te (Ref. 40) and Bi,[41] where independent chemical potentials are used for electrons and holes. The use of a single chemical potential reflects the expected ultrafast rate of impact ionization and Auger recombination in a dense electron-hole plasma. Exchange and correlation are included through the use of the local density approximation in the formulation of Perdew and Wang.[42] Wave functions are treated as an expansion of plane waves up to an energy cutoff of 30 Hartree. Pseudopotentials are of the Troullier–Martins type,[43] with $4d$, $5s$, and $5p$ electrons being treated as valence for In, and $5s$ and $5p$ electrons being treated as valence for Sb. Calculations are performed for the two atom irreducible unit cell. For all calculations except where otherwise specified, Brillouin zone sampling is performed on a set of four shifted $6\times6\times6$ Monkhorst–Pack $\vec{k}$ point grids.[44] Optimization of the lattice parameter at $T=0$ K leads to a calculated equilibrium value of 6.425 Å, whereas the experimental value is 6.479 Å.[45] Electronic density of states for use in determining carrier densities is performed on a set of four shifted $16\times16\times16$ Monkhorst–Pack $\vec{k}$ point grids. The calculated electronic density of states are in good agreement with those of Chelikowsky and Cohen.[46,47] Carrier densities for a given electronic temperature are calculated as an integral over the conduction band density of states with the assumption of a Fermi–Dirac distribution.[48] Dynamical matrices are calculated at 16 unique $\vec{q}$ vectors in the irreducible Brillouin zone and are interpolated to obtain lattice dynamical information. Lattice dynamics information is calculated on an $88\times88\times88$ grid of evenly spaced points in the Brillouin zone. Due to symmetry considerations, these points can be reduced to a unique set of 8119 $\vec{q}$ points.

III. RESULTS

A. Phonon dispersion

The phonon dispersion relation for three high symmetry directions in reciprocal space was calculated at 15 different

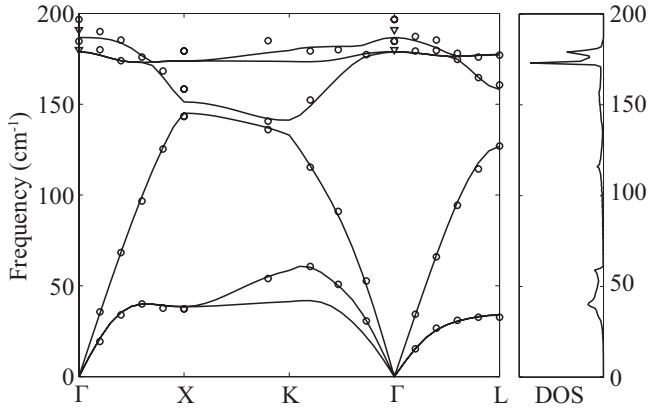

FIG. 1. Phonon dispersion and phonon density of states calculated at an electronic temperature of $T=0$ K, corresponding to 0% carrier density. Also shown are data obtained by neutron (○, Ref. 49) and Raman (▽, Ref. 50) scattering at room temperature.

electronic temperatures, corresponding to 15 carrier density values to determine the effects of carrier density on lattice stability. The ground state phonon dispersion calculated at $T=0$ K is displayed in Fig. 1, corresponding to 0% carrier density. Figure 1 also shows neutron[49] and Raman[50] scattering data collected at ~300 K.

Increasing the carrier density from the unexcited ground state by increasing the electronic temperature leads to softening of all phonon modes. Eventually, the transverse acoustic (TA) phonon at the zone boundary in the (100) direction (X point) becomes unstable around a carrier density of 3.7%, as shown in Fig. 4. The onset of the instability at the X point differs from calculations on silicon, where the instability develops first at the L point.[17,20,22] Figure 2 shows the phonon dispersion curves for a carrier density of 4.0%. Note that the TA phonon at the X point is strongly destabilized, while the other principal direction zone boundary TA phonon frequencies remain real valued. Exciting even higher numbers of carriers leads to a destabilization of the TA modes over the entire Brillouin zone. The phonon dispersion for such an

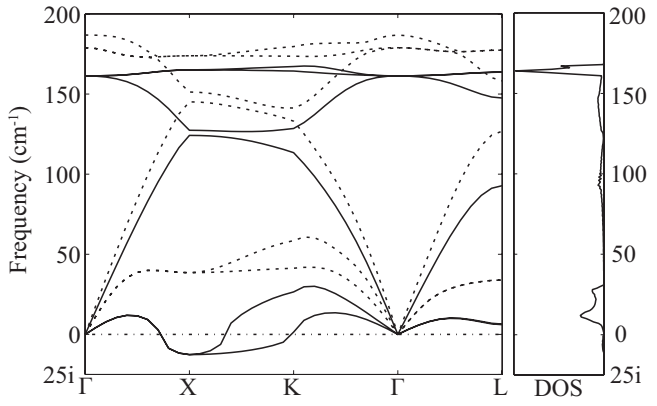

FIG. 2. Phonon dispersion and phonon density of states calculated at an electronic temperature of $T=9450$ K, corresponding to 4.0% carrier density (solid). Also shown are $T=0$ K data for reference (dashed). The TA phonon at the X point is strongly destabilized, with an imaginary frequency, while other zone boundary TA phonons are softened, but not unstable.

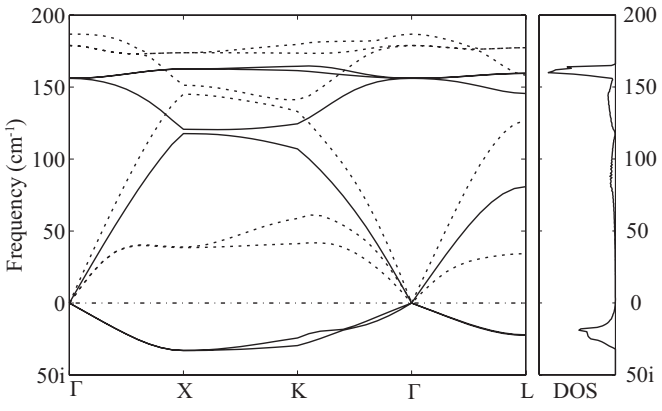

FIG. 3. Phonon dispersion and phonon density of states calculated at an electronic temperature of $T=12\,500$ K, corresponding to 6.6% carrier density. Also shown are $T=0$ K data for reference (dashed). The entire TA branch is now unstable, indicating a loss of shear restoring forces.

instance is depicted in Fig. 3, which is calculated at 6.6% carrier density.

Figure 4 presents the carrier density dependent TA phonon frequencies at three different high symmetry points to indicate the directionality of the lattice instability. Consistent with previous theory on Si,[17,18] the instability develops over a narrow carrier density range for all high symmetry directions.

B. Diffraction model

To compare the calculations with experimental x-ray diffraction data, we develop a model for predicting the time-dependent diffraction intensity from the lattice dynamics calculations. A time-dependent Debye–Waller model is employed, similar to that used in prior analysis of time-resolved x-ray diffraction data.[31–33] In formulating this model, we begin by expressing the diffraction intensity from a perfect polyatomic lattice as the square modulus of the structure factor, F,[51]

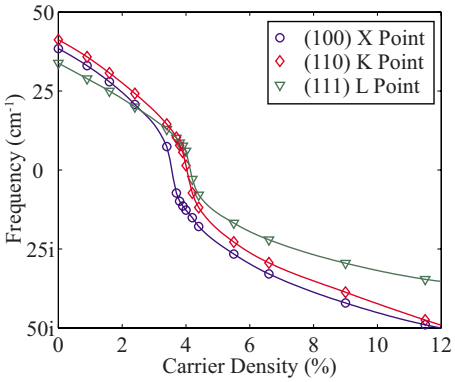

FIG. 4. (Color online) TA phonon frequencies at zone boundaries in the (100) direction (X point) (○), (111) direction (L point) (▽), and lowest energy phonon in the (110) direction (K point) (◇) as a function of carrier density. Lines are provided to guide the eye.

$$F = \sum_{\kappa} f_{\kappa} e^{i\vec{Q}\cdot\vec{r}_{\kappa}}. \quad (1)$$

In Eq. (1), the sum is performed over κ, all the atoms in the unit cell, f_{κ} represents the atomic scattering factor, $\vec{Q}$ the scattering vector, and $\vec{r}_{\kappa}$ the position of the atom in the unit cell. Conventional diffraction theory then introduces a Debye–Waller factor, $e^{-M_{\kappa}}$, to account for thermal vibrational motion of the atoms around their equilibrium positions.[51] In the model presented here, the Debye–Waller factor is modified to account for time-dependent disordering, producing a time-dependent structure factor,

$$F(t) = \sum_{\kappa} f_{\kappa} e^{-M_{\kappa}(t)} e^{i\vec{Q}\cdot\vec{r}_{\kappa}}. \quad (2)$$

Preliminary calculations indicate that promoting free carriers does not displace the equilibrium position of the atoms in the unit cell and, therefore, $\vec{r}_{\kappa}$ is not a time-dependent quantity. For the diatomic primitive unit cell of InSb, the time-dependent diffraction intensity in the kinematic limit is proportional to

$$I(t) \propto \left| f_{\mathrm{In}} e^{-M_{\mathrm{In}}(t)} + f_{\mathrm{Sb}} e^{-M_{\mathrm{Sb}}(t)} e^{i\vec{Q}\cdot\vec{r}_{\mathrm{Sb}}} \right|^2. \quad (3)$$

To use this expression for predicting x-ray diffraction profiles, the time-dependent Debye–Waller factors must be produced from the lattice dynamical information. Equation (4) presents the results of the well established procedure for calculating thermal Debye–Waller factors,[51]

$$M_{\kappa} = \sum_{l,\vec{q}} \frac{\hbar}{2Nm_{\kappa}\omega} \left(n_{l,\vec{q}} + \frac{1}{2} \right) |\vec{Q}\cdot\vec{\epsilon}_{l,\vec{q}}|^2. \quad (4)$$

The summation in Eq. (4) is over all wave vectors $\vec{q}$ and modes l, and N is the number of $\vec{q}$ points, m_{κ} the mass of the ion, ω the phonon frequency, $n_{l,\vec{q}}$ the thermal occupation, and $\vec{\epsilon}_{l,\vec{q}}$ the phonon polarization vector. This thermal Debye–Waller factor can be modified to include the effects of time-dependent impulsive softening of phonon frequencies as follows:

$$M_{\kappa}(t) = \sum_{l,\vec{q}} \frac{W(\vec{q})}{\Sigma_{\vec{q}} W(\vec{q})} \left(\frac{k_B T}{4m\omega^i_{l,\vec{q}}\omega^f_{l,\vec{q}}} \right) |\vec{Q}\cdot\vec{\epsilon}^{\,f}_{l,\vec{q}}|^2 \times \left\{ \frac{\omega^f_{l,\vec{q}}}{\omega^i_{l,\vec{q}}} [1+\cos(2\omega^f_{l,\vec{q}}t)] + \frac{\omega^i_{l,\vec{q}}}{\omega^f_{l,\vec{q}}} [1-\cos(2\omega^f_{l,\vec{q}}t)] \right\}. \quad (5)$$

In deriving this expression, the high temperature approximation for the phonon occupation has been made (InSb has a Debye temperature of 175 K[52]). Furthermore, k_B is Boltzmann's constant, $\omega^i_{l,\vec{q}}$ the initial phonon frequency for a given mode and $\vec{q}$ point, $\omega^f_{l,\vec{q}}$ the corresponding softened phonon frequency, and $\epsilon^f_{l,\vec{q}}$ the phonon polarization vector for the softened phonon. The initial term in Eq. (5) is inserted so that the expression can be used with the $\vec{q}$ point sampling in the DFPT calculations. The value of $W(\vec{q})$ corresponds to the number of symmetrically equivalent $\vec{q}$ points that each unique $\vec{q}$ point corresponds to in the calculation. Therefore, the initial term represents a weighting scheme to account for the symmetry of the system.[62]

The system is initially assumed to be in thermal equilibrium at room temperature by using $\omega^i_{l,\vec{q}}$ calculated at $T=0$ K. Phonon frequencies calculated at the other electronic temperatures are used for $\omega^f_{l,\vec{q}}$ with the phonon occupation remaining the same for each band and $\vec{q}$ point. Following the increase in the electronic temperature and the resultant changes in the phonon dispersion, the unchanged phonon population no longer corresponds to a well-defined vibrational temperature. This formulation will be used in Sec. IV to calculate time-dependent diffraction intensities for comparison with experiment.

The theoretical calculations and the Debye–Waller model presume a harmonic interatomic potential or small displacements from the average position. While clearly an oversimplification of the true potential, a harmonic description provides an accurate representation of structural dynamics for times short compared to the phonon-phonon and electron-phonon scattering times. Instantaneous normal mode descriptions of the dynamics in liquids demonstrate the validity of using a harmonic potential to describe the ultrafast structural dynamics of inherently anharmonic systems.[53,54] For the case of room temperature InSb, such a model should be applicable for at most a half of a picosecond, which is the time required to move half the nearest neighbor distance with a room temperature rms velocity.

C. Carrier density estimation

Hillyard *et al.*[33] developed a simple method for estimating the carrier density to facilitate the qualitative comparison of theory and experiment. As we demonstrate in Sec. IV, this method for estimating the carrier density leads to large discrepancies between the calculated and experimental carrier density dependence of the structural dynamics. This deviation between theory and experiment appears to result primarily from inaccuracies in the carrier density estimation. We have modified the method for estimating the carrier density to account for time-dependent changes in the reflectivity, which results in qualitative agreement between theory and experiment. This method will be briefly discussed before addressing the calculations in the context of experimental measurement.

Hillyard *et al.*[33] used the parameters of Rousse *et al.*[29] to determine the absorbed laser energy density in a volume defined by the 95% x-ray penetration depth. For the data of Hillyard *et al.*, the x-ray probe depth was absorption limited and determined by the x-ray incidence angles of 0.3°, 0.35°, and 0.4°, which correspond to 95% penetration depths of 50, 100, and 140 nm, respectively.[55] The authors then used the InSb electronic density of states and a Fermi–Dirac distribution to determine the electronic temperature and resultant carrier density needed to create an equivalent electronic energy density.[48] The method does not account for the change in optical reflectivity induced by laser absorption. This leads to an overestimation of the carrier density, particularly at high laser fluences where the leading edge of the pulse has the potential to modify the optical properties of the crystal prior to the arrival of later portions of the laser pulse.

Sokolowski-Tinten *et al.* measured these effects for silicon and determined that the enhancement of the material's

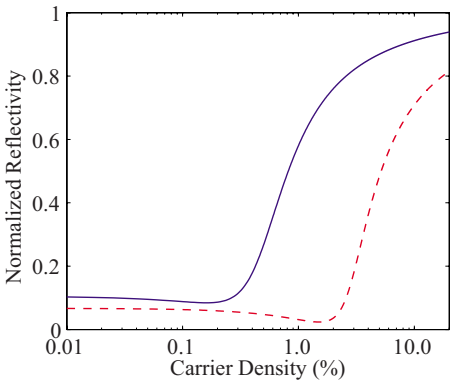

FIG. 5. (Color online) Reflectivity (p-polarized and 65° incidence with respect to the surface normal) as a function of carrier density, calculated as described in the text. The solid line represents InSb and the dashed line represents Si. The lower band gap and optical effective mass move the InSb curve to lower carrier densities and will cause increases in reflectivity at lower carrier densities as compared with Si.

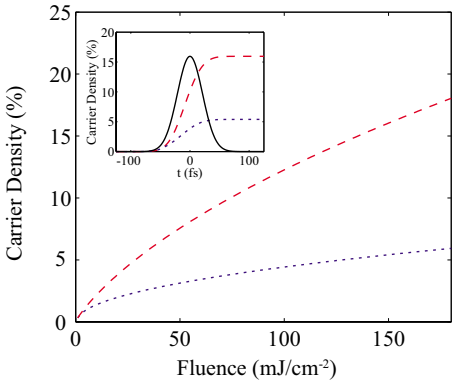

FIG. 6. (Color online) Carrier density as a function of incident laser fluence, using the Drude model for reflectivity (dot) and a constant reflectivity of 0.1 (dash). Carrier densities are calculated over the 140 nm x-ray probe depth for 0.4° x-ray incidence and 65° laser incidence with respect to the surface normal. The inset displays the generated carrier density as a function of time for a 150 mJ/cm^2, 50 fs FWHM pulse, overlayed with the pulse profile in arbitrary units (solid).

reflectivity on an ultrafast time scale results predominantly from the laser excited free carriers and demonstrated that this response can be accurately approximated by the Drude model. Following this prescription, we use the Drude model to estimate the influence of transient reflectivity on the absorbed laser fluence. The complex dielectric function is equal[56] to

$$\epsilon_{mod} = \epsilon_g - \frac{N_{e-h}e^2}{\epsilon_0 m^*_{opt} m_e \omega^2} \frac{1}{1 + i\frac{1}{\omega\tau_D}}. \quad (6)$$

In this expression, ϵ_g is the dielectric constant in the absence of photoexcitation, which is $19.105+i5.683$ at 1.5 eV for InSb.[57] $N_{e\text{-}h}$ is the photoexcited carrier density, e the charge of an electron, ϵ_0 the permittivity of free space, and ω the frequency of light used in the photoexcitation process. The optical effective mass of the carriers m^*_{opt}, as defined by Sokolowski-Tinten *et al.*,[56] is calculated by using published values of effective mass parameters.[58] The Drude damping time τ_D is taken to be 1 fs.[56] By using Eq. (6), the modified reflectivity for InSb and Si are calculated and appear in Fig. 5 for the experimental conditions of Hillyard *et al.* (p polarization and 65° incidence with respect to the surface normal).

As is evident upon examination of the figure, the InSb curve is shifted to lower carrier densities than the Si curve due to its smaller band gap and lower effective masses. A qualitative interpretation suggests that time-dependent increases in the reflectivity will be stronger in InSb than in Si, as the onset of reflectivity enhancement occurs at much lower carrier density. The electron-hole plasma generated by the leading edge of the laser pulse will increase the reflectivity for the trailing edge of the pulse, reducing the absorbed laser energy. This analysis assumes that the electronic excitations equilibrate much faster than the duration of the laser pulse. This assumption is reasonable, given that a significant fraction of the electronic equilibration will occur on a sub-10-fs time scale,[59] and also consistent with the use of a single chemical potential in the theoretical calculations.

To apply this model to the data, we calculate carrier densities for two limiting conditions. First, we assume a constant reflectivity of 0.1, which is consistent with prior analysis. In the second analysis, we assume that electronic relaxation occurs much faster than the laser pulse duration. For this case, the electronic system is instantly equilibrated to the Fermi–Dirac distribution consistent with the absorbed energy, and then this time-dependent carrier density is used to calculate a time-dependent reflectivity. Figure 6 shows the laser fluence dependence of the mean carrier density for these limiting conditions. The pulse profile is depicted in arbitrary units in the inset of Fig. 6. These calculations show that the reflectivity rapidly increases in the same carrier density range that the phonon dispersion curves rapidly soften. This will have the effect of decreasing the number of carriers excited for a given increase in laser fluence in the range where the lattice stability is most sensitive to carrier density. This result is relevant to the experimental measurements independent of the detailed electron dynamics as long as this critical carrier density range is created during the laser pulse duration.

Before calculations and experiment can be compared, the validity and limitations of this comparison should be addressed. The nonuniformity of the experimentally generated and probed carrier density distinguishes experiment from theoretical calculation. The nonlinear absorption of the laser pulse results in a large carrier density gradient within the first hundred nanometers of InSb, though ambipolar carrier diffusion will greatly reduce this gradient before significant atomic motion has occurred.[60,61] For x-ray probe depths comparable to or deeper than the laser penetration depth, x-ray diffraction will measure the crystal response for a range of carrier densities. This carrier density averaging that occurs for a given laser fluence and x-ray incidence angle makes an accurate quantitative comparison between experiment and theory impossible. Nonetheless, trends can be established and average carrier densities estimated so that qualitative comparisons can be achieved.

IV. DISCUSSION

Section III A presents density functional perturbation theory calculations of the phonon dispersion curves of InSb as a function of electronic temperature. In Sec. III B, a formulation to transform these quasiequilibrium lattice dynamics calculations into time-dependent diffraction intensities has been presented. The information contained in the calculations of Sec. III A can now be used with Eqs. (3) and (5) to produce temporal diffraction profiles, which can be compared to the experimentally measured diffraction transients initiated by an intense laser excitation.

Predicted time-dependent diffraction intensities are calculated by using the phonon frequencies and polarization vectors obtained from the DFPT lattice dynamics results. Figure 7(a) presents the temporal diffraction profiles for 3.7%, 5.5%, and 9.0% carrier densities, probing at the (111) Bragg peak. Also shown for comparison purposes are data collected at 130 mJ/cm^2 ($\approx$5% carrier density) excitation fluence from Gaffney *et al.*[32] and a 410 fs full width at half maximum (FWHM) Gaussian, representing constant rms velocity disordering. Figure 7(b) shows the same curves and data for the (220) Bragg peak. In this case, the Gaussian representing inertial dynamics is a 250 fs Gaussian. All curves shown are convolved with a 180 fs FWHM Gaussian to account for the temporal instrument response of the experimental data.[33]

The predicted diffraction intensities for lower carrier densities show a decrease in intensity due to phonon softening followed by a partial recovery, with recurrences in the diffracted intensity extending beyond the 1 ps time delay shown. This effect will not be present in the experimental data due to effects that have not been considered in the model presented above, such as atomic collisions, carrier diffusion and recombination, vibrational heating, and phonon-phonon scattering. Upon increasing the carrier density, the destabilization of the potential energy surface becomes evident as the disordering times become increasingly shorter. For both the (111) and (220) Bragg peaks, the calculated diffraction profiles at 5.5% carrier density are consistent at early times with the 130 mJ/cm^2 ($\approx$5% carrier density) time-dependent diffraction data from Gaffney *et al.*[32] These calculated diffraction curves show nearly constant velocity dynamics for time delays less than 500 fs, which is consistent with experimental observations. Deviations between experiment and theory at later times are attributed to the effects mentioned above that are not included in this model.

A uniformly softened Debye model for the phonon dispersion of laser-excited InSb also provides similar time-dependent diffraction curves to those presented in Fig. 7.[33] Despite the significantly different phonon dispersions used in the models, we obtain similar results due to the integration over all phonon modes in Eq. (5). This integration makes the time-dependent Debye–Waller insensitive to the details of the phonon dispersion. While the Debye model generates qualitatively similar results, they cannot be directly compared to experiment because they cannot be correlated with carrier density or laser fluence. This represents a significant advantage for the more thorough theoretical approach presented in this paper.

As noted in the Introduction, previous theoretical work indicated that the lattice instability in Si should first develop

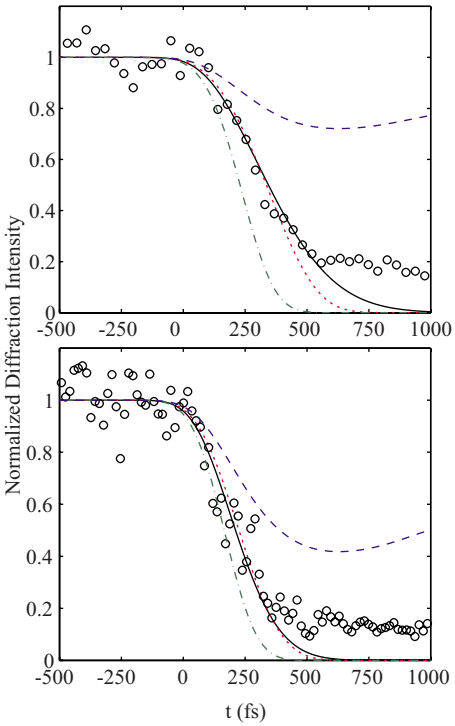

FIG. 7. (Color online) (a) Predicted time-dependent (111) diffraction intensity for InSb at carrier densities of 3.7% (dash), 5.5% (dot), and 9.0% (dash-dot), shown with data collected at 130 mJ/cm^2 ($\approx$5% carrier density) fluence from Gaffney *et al.* (Ref. 32) ($\bigcirc$) and a 410 fs FWHM Gaussian (solid), representing the time scale for inertial dynamics probed at the (111) Bragg peak at room temperature (Ref. 31). (b) Predicted time-dependent (220) diffraction intensity for carrier densities of 3.7% (dash), 5.5% (dot), and 9.0% (dash-dot), shown with data collected at 130 mJ/cm^2 ($\approx$5% carrier density) fluence from Gaffney *et al.* (Ref. 32) ($\bigcirc$) and a 250 fs FWHM Gaussian (solid), representing the time scale for inertial dynamics probed at the (220) Bragg peak at room temperature (Ref. 31). All curves have been convolved with a 180 fs FWHM Gaussian representing the instrument response.

for acoustic phonons transverse at the L point, leading to an anisotropy in the disordering, with motion in directions transverse to the $\langle 111 \rangle$ occurring faster than motion in the $\langle 111 \rangle$ direction.[17,20] This prediction is at odds with the experimental finding of Gaffney *et al.* for InSb, where rms displacements increase faster when projected along the (111) direction than along the (110) direction.[32] To compare the present work with earlier theory and experiment, time-dependent rms displacements projected on a specific lattice vector are obtained as $u^Q_{rms}(t) = \sqrt{-\ln[I(t)]/Q^2}$, where $I(t)$ is the normalized time-dependent diffraction intensity. Time-dependent changes in rms displacements projected along the (111) and (110) directions, $\Delta u^Q_{rms}(t)$, are extracted for InSb and found to be isotropic. Figure 8 displays this predicted rms displacement, along with data from Gaffney *et al.* collected at an excitation fluence of 130 mJ/cm^2 ($\approx$5% carrier density).[32]

As noted above, the calculated displacement curves are not able to reproduce the anisotropy observed by Gaffney *et al.* after constant velocity disordering.[32] This is most likely due to the fact that the model presented here only accounts

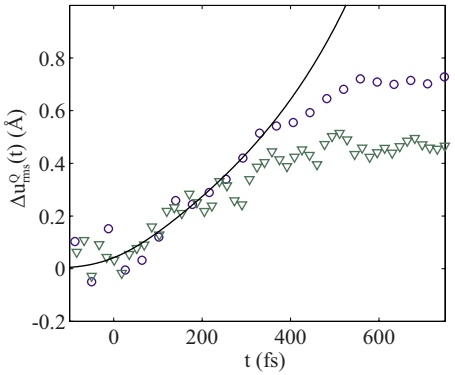

FIG. 8. (Color online) Time-dependent root-mean-square displacement (solid) for a carrier density of 5.5% calculated as described in the text, convolved with a 180 fs FWHM Gaussian representing the instrument response. Displacements were found to be isotropic in the ⟨111⟩ and ⟨110⟩ directions. Symbols represent experimental data collected at 130 mJ/cm^2 (≈5% carrier density) from Ref. 32 for the ⟨111⟩ (○) and ⟨110⟩ (▽) directions.

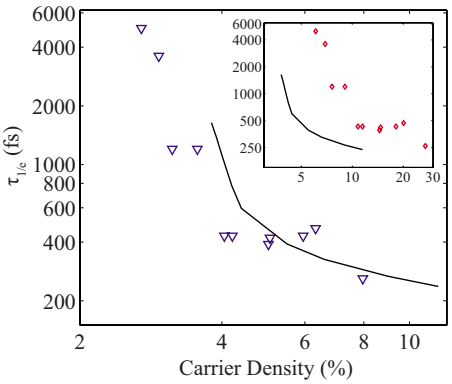

FIG. 9. (Color online) Time for the normalized diffraction intensity to drop to $1/e$ is displayed as a function of the carrier density. The theoretical data points are calculated within the time-dependent Debye–Waller model by using the DFPT lattice dynamical data and are displayed as a solid line. The experimental data points are from Hillyard *et al.* (Ref. 33), with carrier densities calculated by using the Drude transient reflectivity model (▽). The inset displays the same solid line, representing the theoretical data points. However, it is compared with the experimental data points plotted with carrier densities calculated by using the constant reflectivity model (○).

for electronically induced softening of the potential energy surface. It does not account for structural dynamics after the onset of collisional dynamics or deviations from a Gaussian distribution of atomic displacements, which would invalidate the assumptions underlying both the experimental and theoretical analysis. Based on the disagreement between data and theory, it can be postulated that the anisotropy observed by Gaffney *et al.* does not arise from the directionality of the electronically induced softening.

The insensitivity of disordering dynamics over a large fluence range was interpreted by Hillyard *et al.* to indicate a potential energy surface that was insensitive to large carrier density changes, a conclusion in contradiction to earlier theoretical work on Si.[33] To compare the experimental data and theory contained in this paper, carrier densities associated with each experimental data point are calculated for the two limiting cases presented in Sec. III C. To facilitate the comparison of theory and experiment, we parameterize the dynamics with a single time constant, $\tau_{1/e}$, the time required for the normalized (111) diffraction intensity to reach a value of $1/e$. In Fig. 9, the $\tau_{1/e}$ values for both the experimental and theoretical data points are plotted for comparison. In the main portion of the figure, the experimental fluences are converted to carrier densities by using the transient reflectivity Drude model. The inset displays the experimental data points plotted versus a carrier density calculated by using the constant reflectivity model.

As seen in Fig. 9, the transient reflectivity model alleviates the large discrepancy between theory and experiment. This improved agreement reflects an idiosyncrasy of InSb; the rate of change in the reflectivity appears to be greatest in the same carrier density range where the crystal dynamics have the greatest carrier density dependence. Hence, the insensitivity of the measured dynamics to large changes in laser fluence appears to result from an inability to couple laser energy into the crystal once a critical carrier density has been achieved. There still exists a regime where the disordering is insensitive to carrier density, though it is much narrower than previously estimated by Hillyard *et al.* It is also evident that the sharp decrease in disordering times occurs at a higher carrier density in the theory as compared to experiment. These effects likely reflect the continued uncertainty about the estimated average carrier density.

V. SUMMATION

Density functional perturbation theory calculations of lattice dynamics as a function of carrier excitation have been performed to assist in the interpretation of ultrafast x-ray diffraction measurements of laser-induced disordering in InSb.[31–33] The calculations qualitatively resemble previous work done on Si, but the lattice instability develops with a directionality distinct from that seen in Si. The anisotropy seen in the calculated phonon dispersion curves does not generate any substantial directional dependence on the time-dependent rms displacement. The summation over all wave vectors $\vec{q}$ that occurs in the calculation of the Debye–Waller factor makes diffraction insensitive to anisotropy in the phonon softening, at least for highly symmetric crystal structures. Time-resolved diffuse scattering would allow one to probe changes in the phonon dispersion at a particular wave vector and could, therefore, be critical in elucidating the precise disordering dynamics. The carrier density dependence of the calculated time-dependent rms displacements also resemble the experimental laser fluence dependence of the disordering dynamics, once the time-dependent optical reflectivity of InSb has been taken into account. The dynamics extracted from these theoretical calculations only account for the impact of electronically driven lattice softening on the time dependent x-ray diffraction intensity, yet they still result in a strong qualitative agreement between theory and experiment. This represents convincing evidence that the initial disordering dynamics generated in InSb by intense laser ex-

citation results predominantly from electronically induced modifications of the potential energy surface.

ACKNOWLEDGMENTS

This research was supported by the U.S. Department of Energy, Office of Basic Energy Science through direct support for SSRL, as well as individual investigators. SSRL is a national user facility operated by Stanford University. Portions of this work were supported by the W.M. Keck Foundation, Stanford University PULSE Center, and University of Michigan FOCUS Center. S. Fahy and E. Murray are acknowledged for helpful conversations on DFPT calculations of lattice dynamics in the presence of excited carriers. The authors thank S. Fahy for a critical reading of the manuscript. A. M. Lindenberg and K. Sokolowski-Tinten are acknowledged for helpful conversations regarding ultrafast disordering processes in covalent semiconductors as well as the effect of electron-hole plasmas on semiconductor reflectivity. We also thank the SPPS collaboration.

*kgaffney@slac.stanford.edu

[1] D. H. Reitze, X. Wang, H. Ahn, and M. C. Downer, Phys. Rev. B **40**, 11986 (1989).
[2] D. H. Reitze, H. Ahn, and M. C. Downer, Phys. Rev. B **45**, 2677 (1992).
[3] K. Sokolowski-Tinten, J. Bialkowski, and D. von der Linde, Phys. Rev. B **51**, 14186 (1995).
[4] K. Sokolowski-Tinten, H. Schulz, J. Bialkowski, and D. von der Linde, Appl. Phys. A: Solids Surf. **53**, 227 (1991).
[5] S. V. Govorkov, I. L. Shumay, W. Rudolph, and T. Schroder, Opt. Lett. **16**, 1013 (1991).
[6] E. N. Glezer, Y. Siegal, L. Huang, and E. Mazur, Phys. Rev. B **51**, 6959 (1995).
[7] Y. Siegal, E. N. Glezer, and E. Mazur, Phys. Rev. B **49**, 16403 (1994).
[8] L. Huang, J. P. Callan, E. N. Glezer, and E. Mazur, Phys. Rev. Lett. **80**, 185 (1998).
[9] E. N. Glezer, Y. Siegal, L. Huang, and E. Mazur, Phys. Rev. B **51**, 9589 (1995).
[10] S. V. Govorkov, T. Schroder, I. L. Shumay, and P. Heist, Phys. Rev. B **46**, 6864 (1992).
[11] J. P. Callan, A. M.-T. Kim, C. A. D. Roeser, and E. Mazur, Phys. Rev. B **64**, 073201 (2001).
[12] P. Saeta, J. K. Wang, Y. Siegal, N. Bloembergen, and E. Mazur, Phys. Rev. Lett. **67**, 1023 (1991).
[13] I. L. Shumay and U. Hofer, Phys. Rev. B **53**, 15878 (1996).
[14] C. V. Shank, R. Yen, and C. Hirlimann, Phys. Rev. Lett. **50**, 454 (1983).
[15] H. W. K. Tom, G. D. Aumiller, and C. H. Brito-Cruz, Phys. Rev. Lett. **60**, 1438 (1988).
[16] I. Stich, R. Car, and M. Parrinello, Phys. Rev. B **44**, 4262 (1991).
[17] R. Biswas and V. Ambegaokar, Phys. Rev. B **26**, 1980 (1982).
[18] P. Stampfli and K. H. Bennemann, Phys. Rev. B **42**, 7163 (1990).
[19] P. Stampfli and K. H. Bennemann, Phys. Rev. B **46**, 10686 (1992).
[20] P. Stampfli and K. H. Bennemann, Phys. Rev. B **49**, 7299 (1994).
[21] D. A. Reis, K. J. Gaffney, G. H. Gilmer, and B. Torralva, MRS Bull. **31**, 601 (2006).
[22] V. Recoules, J. Clerouin, G. Zerah, P. M. Anglade, and S. Mazevet, Phys. Rev. Lett. **96**, 055503 (2006).
[23] T. Dumitrica and R. E. Allen, Phys. Rev. B **66**, 081202(R) (2002).
[24] T. Dumitrica, A. Burzo, Y. Dou, and R. E. Allen, Phys. Status Solidi B **241**, 2331 (2004).
[25] P. L. Silvestrelli, A. Alavi, M. Parrinello, and D. Frenkel, Phys. Rev. Lett. **77**, 3149 (1996).
[26] P. L. Silvestrelli, A. Alavi, M. Parrinello, and D. Frenkel, Phys. Rev. B **56**, 3806 (1997).
[27] K. J. Gaffney and H. N. Chapman, Science **316**, 1444 (2007).
[28] C. W. Siders, A. Cavalleri, K. Sokolowski-Tinten, C. Toth, T. Guo, M. Kammler, M. H. von Hoegen, K. R. Wilson, D. von der Linde, and C. P. J. Barty, Science **286**, 1340 (1999).
[29] A. Rousse *et al.*, Nature (London) **410**, 65 (2001).
[30] K. Sokolowski-Tinten, C. Blome, C. Dietrich, A. Tarasevitch, M. Horn von Hoegen, D. von der Linde, A. Cavalleri, J. Squier, and M. Kammler, Phys. Rev. Lett. **87**, 225701 (2001).
[31] A. M. Lindenberg *et al.*, Science **308**, 392 (2005).
[32] K. J. Gaffney *et al.*, Phys. Rev. Lett. **95**, 125701 (2005).
[33] P. B. Hillyard *et al.*, Phys. Rev. Lett. **98**, 125501 (2007).
[34] S. Baroni, S. de Gironcoli, A. D. Corso, and P. Giannozzi, Rev. Mod. Phys. **73**, 515 (2001).
[35] X. Gonze and C. Lee, Phys. Rev. B **55**, 10355 (1997).
[36] X. Gonze, Phys. Rev. B **55**, 10337 (1997).
[37] X. Gonze *et al.*, Comput. Mater. Sci. **25**, 478 (2002).
[38] A. Alavi, J. Kohanoff, M. Parrinello, and D. Frenkel, Phys. Rev. Lett. **73**, 2599 (1994).
[39] E. S. Zijlstra, L. L. Tatarinova, and M. E. Garcia, Phys. Rev. B **74**, 220301(R) (2006).
[40] P. Tangney and S. Fahy, Phys. Rev. B **65**, 054302 (2002).
[41] E. D. Murray, S. Fahy, D. Prendergast, T. Ogitsu, D. M. Fritz, and D. A. Reis, Phys. Rev. B **75**, 184301 (2007).
[42] J. P. Perdew and Y. Wang, Phys. Rev. B **45**, 13244 (1992).
[43] N. Troullier and J. L. Martins, Phys. Rev. B **43**, 1993 (1991).
[44] H. J. Monkhorst and J. D. Pack, Phys. Rev. B **13**, 5188 (1976).
[45] V. G. Giesecke and H. Pfister, Acta Crystallogr. **11**, 369 (1958).
[46] J. R. Chelikowsky and M. L. Cohen, Phys. Rev. B **14**, 556 (1976).
[47] J. R. Chelikowsky and M. L. Cohen, Phys. Rev. B **30**, 4828 (1984).
[48] M. Combescot and J. Bok, J. Lumin. **30**, 1 (1985).
[49] D. L. Price, J. M. Rowe, and R. M. Nicklow, Phys. Rev. B **3**, 1268 (1971).
[50] A. Pinczuk and E. Burstein, Phys. Rev. Lett. **21**, 1073 (1968).
[51] B. E. Warren, *X-Ray Diffraction* (Dover, New York, 1990).
[52] G. Arnold and N. Nereson, Phys. Rev. **131**, 2098 (1963).
[53] R. M. Stratt and M. H. Cho, J. Chem. Phys. **100**, 6700 (1994).
[54] R. M. Stratt, Acc. Chem. Res. **28**, 201 (1995).

[55] B. L. Henke, E. M. Gullikson, and J. C. Davis, At. Data Nucl. Data Tables **54**, 181 (1993).
[56] K. Sokolowski-Tinten and D. von der Linde, Phys. Rev. B **61**, 2643 (2000).
[57] D. E. Aspnes and A. A. Studna, Phys. Rev. B **27**, 985 (1983).
[58] *Semiconductors: Group IV Elements and III-V Compounds*, edited by O. Madelung (Springer-Verlag, Berlin, 1991).
[59] W. H. Knox, D. S. Chemla, G. Livescu, J. E. Cunningham, and J. E. Henry, Phys. Rev. Lett. **61**, 1290 (1988).
[60] J. F. Young and H. M. van Driel, Phys. Rev. B **26**, 2147 (1982).
[61] E. J. Yoffa, Phys. Rev. B **21**, 2415 (1980).
[62] In the process of symmetry reducing the $\vec{q}$ point grid, the resulting $\vec{q}$ points are confined to the positive quadrant of the Brillouin zone. Equation (5) assumes phonon polarization vectors from the entire Brillouin zone, not just the positive quadrant. To account for this, the projection of positive quadrant phonon polarization vectors for a given scattering vector is averaged over all symmetrically equivalent scattering vectors.
[63] http://www.abinit.org